



저작자표시-비영리-변경금지 2.0 대한민국

이용자는 아래의 조건을 따르는 경우에 한하여 자유롭게

- 이 저작물을 복제, 배포, 전송, 전시, 공연 및 방송할 수 있습니다.

다음과 같은 조건을 따라야 합니다:



저작자표시. 귀하는 원저작자를 표시하여야 합니다.



비영리. 귀하는 이 저작물을 영리 목적으로 이용할 수 없습니다.



변경금지. 귀하는 이 저작물을 개작, 변형 또는 가공할 수 없습니다.

- 귀하는, 이 저작물의 재이용이나 배포의 경우, 이 저작물에 적용된 이용허락조건을 명확하게 나타내어야 합니다.
- 저작권자로부터 별도의 허가를 받으면 이러한 조건들은 적용되지 않습니다.

저작권법에 따른 이용자의 권리는 위의 내용에 의하여 영향을 받지 않습니다.

이것은 [이용허락규약\(Legal Code\)](#)을 이해하기 쉽게 요약한 것입니다.

[Disclaimer](#)

# Textured Antireflection Sticker Film for Efficient Solar Cells

Sojeong Lee

Department of Energy Engineering  
(Energy Engineering)

Graduate School of UNIST


# Textured Antireflection Sticker Film for Efficient Solar Cells

A thesis  
submitted to the Graduate School of UNIST  
in partial fulfillment of the  
requirements for the degree of  
Master of Science

Sojeong Lee

01. 16. 2017

Approved by



Advisor

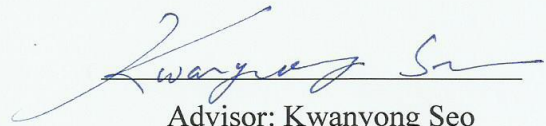
Kwanyong Seo

Textured Antireflection Sticker Film  
for Efficient Solar Cells

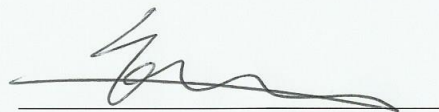
Sojeong Lee

This certifies that the thesis of Sojeong Lee is approved.

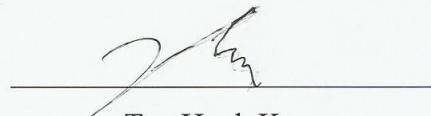
01. 16. 2017



Advisor: Kwanyong Seo



Hyun-Kon Song



Tae-Hyuk Kwon

## **Abstract**

For highly efficient solar cell, it is necessary to understand all the light loss in the solar cell and develop broadband light harvesting. This thesis reports a polydimethylsiloxane (PDMS) film composed of random sized inverted pyramidal structure (RSIPS) fabricated by simple and cheap process that displays excellent optical properties. The RSIPS-PDMS film shows high optical haze which increase the light scattering and low reflection because of a linear grading of the effective refractive index profile from the air to glass or silicon layer. By applying the RSIPS-PDMS on Si solar cell, the current density and efficiency was improved (i.e.,  $35.9\text{mA}/\text{cm}^2$ , 16%) compared to those of reference device (i.e.,  $33.1\text{mA}/\text{cm}^2$ , 14.9%). Also, a polymer solar cell (PSC) with RSIPS-PDMS film has improved current density and efficiency. The RSIPS-PDMS film is suitable for an antireflection film of diverse solar cells.



## Contents

<b>I. Introduction</b> -----	1
1.1 Background of Solar Cells -----	1
1.1.1 Development of Solar Cells -----	1
1.1.2 Principle and Characterization of Solar Cells -----	1
1.1.3 Type of Solar Cells -----	5
1.2 Optical Properties -----	5
1.2.1 Optical Losses -----	5
1.2.2 Antireflection Coatings (ARC) -----	7
1.3 Soft lithography -----	9
1.3.1 Polydimethylsiloxane (PDMS) -----	9
1.3.2 Self-Assembled Monolayers (SAMs) treatment -----	11
1.3.3 Trend of soft lithography -----	13
<b>II. Results and Discussion</b> -----	14
2.1 Random-Sized Inverted Pyramidal Structure (RSIPS) in PDMS film-----	14
2.2 Optical properties -----	17
2.3 Surface wettability and self-cleaning effect -----	26
2.4 Characteristics of the Polymer solar cells -----	29
2.5 Characteristics of the Si solar cells -----	33
2.6 Conclusion -----	38
<b>III. Experimental Section</b> -----	39
3.1 Fabrication of Random-Sized Pyramidal Structured Si mold -----	39
3.2 Fabrication of RISPS-PDMS film -----	39
3.3 Fabrication of Polymer solar cells -----	41
3.3 Fabrication of Si solar cells -----	41
<b>References</b> -----	42
<b>Acknowledgement</b> -----	46

## List of Figures

**Figure 1.1** A J-V curve of solar cells

**Figure 1.2** The optical loss in a solar cell.

**Figure 1.3** Diagram of rays at (a) a single layer on substrate, (b) multilayer on substrate

**Figure 1.4** Process of soft lithography

**Figure 1.5** (a) A diagram of deposition of silane SAM on Si wafer, (b) The basic structure of silane coupling agent.

**Figure 2.1** Schematic images of the soft imprint lithography process steps for random sized inverted pyramidal structures (RSIPS) on PDMS films. The RSIPS-PDMS films was laminated on transparent glass substrate.

**Figure 2.2** (a) cross-sectional and 30°-tilted view SEM image of the (a) RSIPS-Si master mold and (b) RSIPS-PDMS film.

**Figure 2.3** (a) Total transmittance and (b) total reflectance of the flat PDMS film, RIPS-PDMS film on glass or Si wafer.

**Figure 2.4** Structure and the variation in refractive index profile with respect to the film depth.

**Figure 2.5** (a) Schematic diagraming and (b) photographs display the logo image as seen through a RSIPS-PDMS film.

**Figure 2.6** (a) Schematic illustration to show the light scattering effect of RSIP-PDMS film when a laser beam( $\lambda=532\text{nm}$ ) passes through the RSIPS-PDMS film. (b) Photo of diffused light.

**Figure 2.7** Diffuse transmittance of the samples (bare glass, RSIPS-PDMS film/glass, flat PDMS film/glass)

**Figure 2.8** (a) Images show the contact angle of the bare glass, flat PDMS film and RSIPS-PDMS film. (b) Photographs of shape for a water droplet on the substrate (bare glass, RSIPS-PDMS film)

**Figure 2.9** Water droplet self-cleaning behavior of RSIPS-PDMS film compared to bare glass

**Figure 2.10** Schematic diagrams of PSC (a)without PDMS film, (b)with flat PDMS film and (c)RSIPS-PDMS film



**Figure 2.11**(a) J-V curve of the PSC with diverse film, (b)EQE measurement of PSC with diverse film

**Figure 2.12** Schematic diagrams of the Si solar cell

**Figure 2.13** (a) J-V curve and (b) EQE measurement of the Si solar cell

**Figure 2.14** (a) Measured total reflectance and (b) IQE calculation of the Si solar

**Figure 3.1** Contact angle of RSPS Si mold and FOTS-treated RSPS Si mold.

## List of Tables

**Table 1.** The value of the average total transmittance and reflectance over wavelength range of 300-1100nm

**Table 2.** Performance of PSCs with the PDMS films

**Table 3.** Performance of Si solar cells with the PDMS films

# I. Introduction

## 1.1 Background of Solar Cells

### 1.1.1 Development of Solar Cells

Increasing demands and global environmental concerns for energy, coupled with continuous progress in renewable energy developments, are offering new opportunities for use of renewable energy resources. Among the renewable energy resources (i.e., tidal power, solar energy, hydroelectric power, geothermal energy, biomass), solar energy is the most inexhaustible, clean and abundant.<sup>1</sup> The solar power obstructed by the earth is approximately  $1.8 \times 10^{11}$  MW. It is a lot of times larger than current rate of whole the consumption. Solar photovoltaic cell technology is one of the best ways to utilize the solar power. Hence there is growing interest for the development of solar energy harvesting in solar cells. Solar cells are robust and simple in design requiring little maintenance, and have greatest advantages as a stand-alone systems that provides microwatts to megawatts of outputs. Thus, they are used for power supplies, water pumpings, solar home systems, space vehicles, satellites, and even megawatt scale power plants. With such enormous applications, the demand for solar power generation is increasing every year.

### 1.1.2 Principle and Characterization of Solar Cells

#### *Photovoltaic effect*

Photovoltaic effect is the concept that a solar cell turns sunlight into electricity. The sunlight is consisted of photons in solar energy. The photons include different amounts of energy corresponding to different wavelengths. They can be absorbed or reflected, or they can pass right through when photons collide a solar cell. The absorbed photons produce electricity.

#### *Principle of Solar Cells*

Process in the operation of a solar cell is that current flows while holes and electrons move in p-type layer and n-type layer when sunlight enters a solar cell composed of p-type and n-type junction.

Under illumination, electron-hole pairs are generated by photons at p-n junction in device. In order to generate electricity, electron-hole pairs are separated immediately by electric field. Then electrons and holes transport to n-type layer and p-type layer, respectively. The photovoltaic power is generated between p-type layer and n-type layer. At this time, when a load is connected to the electrodes at both ends, a current flows.<sup>2</sup>

### *Characterization of Solar Cells*

The short-circuit current ( $I_{SC}$ ) is the maximum current when the voltage of the solar cell is zero. The  $I_{SC}$  is caused by generation and collection of photogenerated carriers. It is the maximum current that can be drawn out by a solar cell because the photogenerated current and the  $I_{SC}$  are the same. The  $I_{SC}$  is affected by various factors such as the area of the solar cell, the number of photons, the optical properties, the spectrum of the incident light, the collection probability.

The open-circuit voltage ( $V_{OC}$ ) is the maximum voltage of the solar cell that occurs when the current is zero, which is the amount of forward bias.

$$V_{OC} = \frac{nkT}{q} \ln \left[ \frac{I_{SC}}{I_0} + 1 \right] \quad (1.1)$$

It can be seen that  $V_{OC}$  depends on  $I_{SC}$  and the saturation current ( $I_0$ ) of the solar cell via the above equation (1.1).  $I_0$  becomes dependent on the recombination of the solar cell and  $V_{OC}$  becomes a measure of the quantity of recombination in the solar cell.  $V_{OC}$  can also be obtained from the carrier concentration.

$$V_{OC} = \frac{kT}{q} \ln \left[ \frac{(N_A + \Delta n)\Delta n}{n_i^2} \right] \quad (1.2)$$

where  $N_A$  is the doping concentration,  $n_i$  is the intrinsic carrier concentration,  $kT/q$  is the thermal voltage,  $\Delta n$  is the excess carrier concentration. In this way,  $V_{OC}$  obtained from the carrier concentration is called ‘implied  $V_{OC}$ ’.

The fill factor (FF) is parameter that determines the maximum power of the solar cell. That is the maximum power ratio of the solar cell with product  $V_{OC}$  of and  $I_{SC}$

$$FF = \frac{V_{max}J_{max}}{V_{OC}I_{SC}} \quad (1.3)$$

Solar cell efficiency ( $\eta$ ) is the most widely used and important factor that indicates performance of

solar cell. The efficiency is defined as equation (1.4)

$$\eta = \frac{J_{sc}V_{oc}FF}{P_{in}} \times 100 \quad (1.4)$$

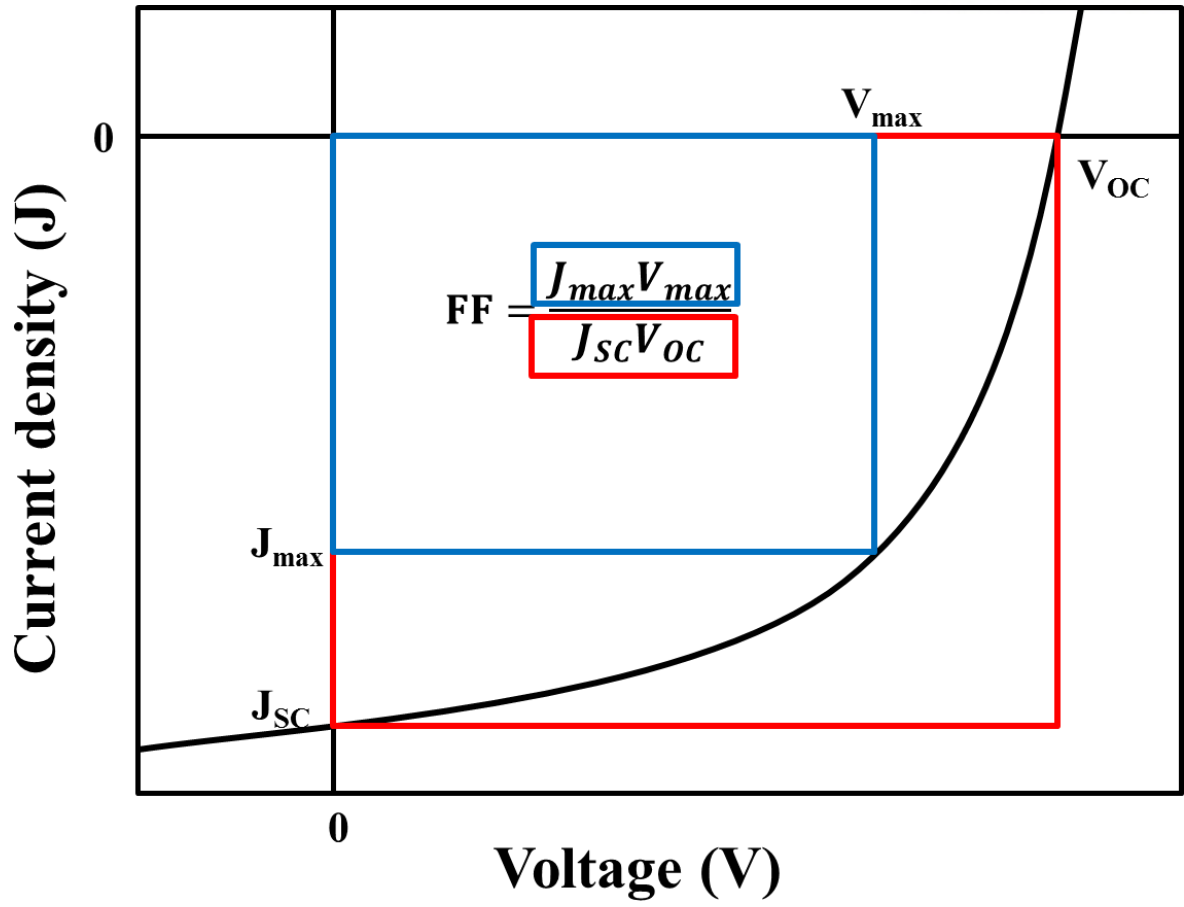


Figure 1.1 A J-V curve of solar cells

### 1.1.3 Type of Solar Cells

#### *Si solar cells*

The first solar cells are mainly based on silicon wafer and it was invented from Bell Lab. The Si based solar cells typically represent a performance of 15-20%. These Si solar cells dominate the market, are commercialized, and can be mainly found on the rooftops. The advantage of this solar cell technology is not only high stability but also excellent performance. However, the Si solar cell are not flexible and require much energy for production.

#### *Polymer solar cells*

Due to the polymer substrate, polymer solar cells (PSC) are usually flexible. The first PSC were invented by Tang et al. at Kodak Research Lab.<sup>3</sup> PSCs are formed from thin films (about 100nm) including polymer. It usually works as a combination of an acceptor (fullerene) and donor (polymer). The PSCs can be fabricated with roll-to-roll technologies and large-scale production. Additionally, these PSCs could be beneficial for some applications because of flexibility and disposability. However, energy conversion efficiencies and stability of PSCs are very low compared to Si solar cell.

## 1.2 Optical Properties

### 1.2.1 Optical Losses

Light that can generate electron-hole pairs entered in the solar cell may be reflected at the surface or not absorbed in the device, and it is called ‘optical loss’. By lowed the short-circuit current, optical losses mainly affect the efficiency of a solar cell. For the almost solar cell, the all visible spectrum (350-800nm) has sufficient energy to generate electron-hole pairs. Thus entire visible light must be absorbed for efficient solar cell.

In case of Si-solar cell, the reflection of a Si surface is about 35% by its high refractive index ( $n_{si}=4.08$ ). The reflectance (R) between two materials (A) is defined by:

$$R = \left( \frac{n_0 - n_{si}}{n_0 + n_{si}} \right)^2$$

where  $n_0$  is A's refractive index and  $n_{si}$  is Si's refractive index.

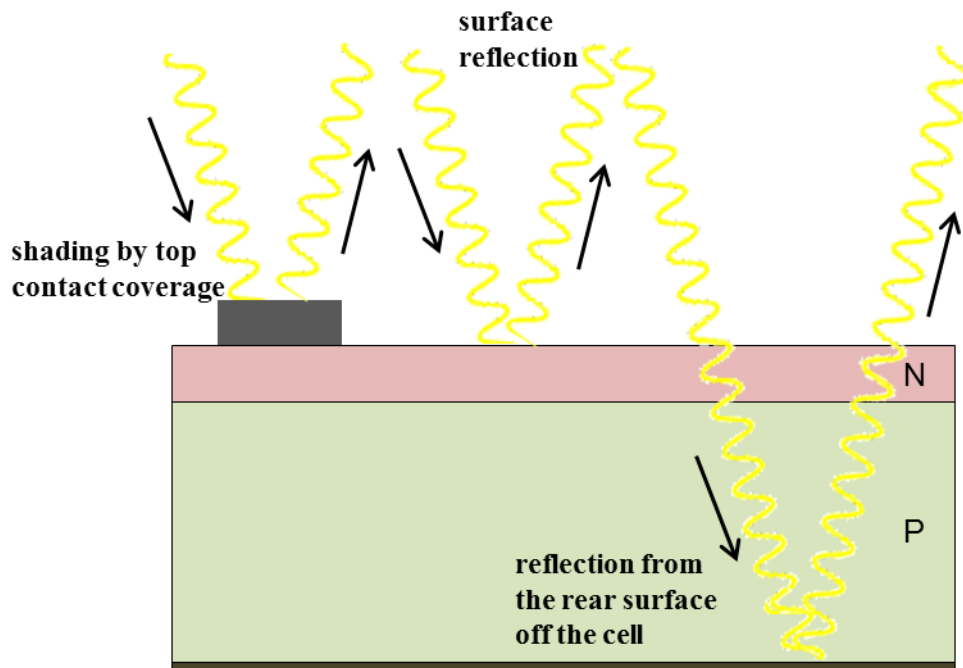


**Figure 1.2** The optical loss in a solar cell.



### 1.2.2 Antireflection Coatings (ARC)

Reducing unwanted light reflections from the material surface is very important for improving the performance of the solar cells. Efforts have been continued to reduce reflectivity by using several coating and diverse patterns on the reflective surface known as ARC. ARC's basic concept was proposed by Rayleigh in 1979 that reflectance from the outer surface of the object can be reduced on condition that the refractive index change between the object and its surrounding medium is small.<sup>4</sup> Over several decades, diverse methods have been followed to reduce the reflection such as thin film coatings and patterning on the surface.<sup>5-6</sup>

#### *Thin film ARC*

The common method of the ARCs is coating a low refractive index layer. When the refractive index and the thickness of the coating should satisfy the sequent conditions, the reflection is zero:

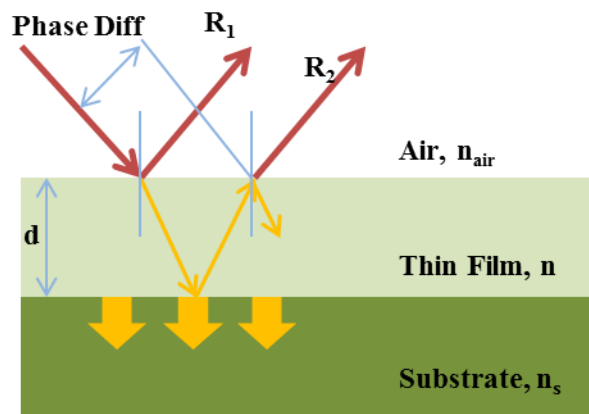
$$n_{arc} = \sqrt{n_0 n_s}$$

$$d_{arc} = \frac{\lambda}{4 \times n_{arc}}$$

where  $n_{arc}$  is the refractive index of ARC and  $n_0$ ,  $n_s$  are the refractive index of the surrounding medium,  $d_{arc}$  is the ARC thickness,  $\lambda$  is the incident light wavelength. The single thin film as ARC is cost effective, simple, and allow the mass production, but it has limitation for angle of incidence and the wavelength.

Also, a multilayer ARC with diverse refractive indices of each layer is suitable for broadband AR, as shown in Figure 1.3.<sup>7-8</sup> However the fabrication processes of the multilayer ARC are complex, costly, and time-consuming.

**a**



**b**

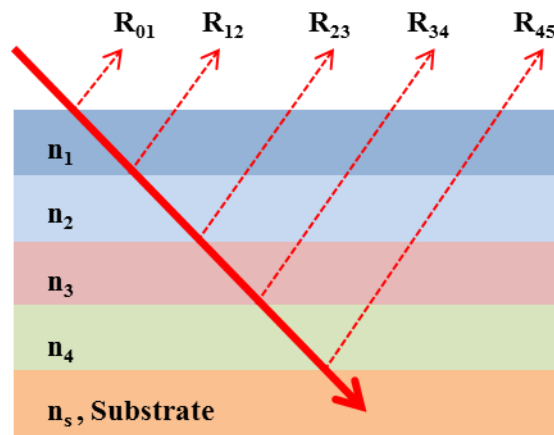


**Figure 1.3** Diagram of rays at (a) a single layer on substrate, (b) multilayer on substrate

### ***Surface Texturing***

Surface texturing also makes the surface antireflective. The roughness of the surface reduces the surface reflection because more light is reflected from the surface than light going out.<sup>9</sup> Over the last several years, many approaches for surface texturing as ARC have been mainly studied in Si inorganic solar cell. These approaches include reactive ion etching (RIE) process,<sup>10-11</sup> replicating fly eyes,<sup>12</sup> heteroepitaxial growth of nanorods,<sup>13</sup> arraying of SiO<sub>2</sub> microspheres.<sup>14</sup> However, it is difficult to apply to different solar cells such as polymer solar cell. Also, the fabrication process for the surface texturing is complex, costly, and inadequate for mass production.

## **1.3 Soft lithography**

Development of an enhanced AR layer by an effective method with simple and cost-effective processes is very important. To fabricate AR layer with nano-and micro-structures, the soft lithographic technique is generally utilized and depends on template replication and self-assembly. It is also a simple process and play crucial role of protective encapsulation for mechanical damage.<sup>15-17</sup> As shown in Figure 1.4, they could be repeatedly utilized for creating a surface pattern transfer, once master molds are fabricated. Moreover, it is suitable for roll-to-roll fabrication and large-scale.<sup>18</sup>

### **1.3.1 Polydimethylsiloxane (PDMS)**

Elastomeric polydimethylsiloxane (PDMS) is the key element in soft lithography for the pattern transfer. It is very useful due to its flexibility, durability, and low free surface energy. In addition to it is appropriate AR layer because the refractive index of PDMS ( $n=1.43$ ) is lower than other substrate such as Si wafer( $n=4.08$ ) or glass( $n=1.5$ ).<sup>19</sup> Additionally, the PDMS layer could be detached from surface of flat substrates as well as strongly attached on it.

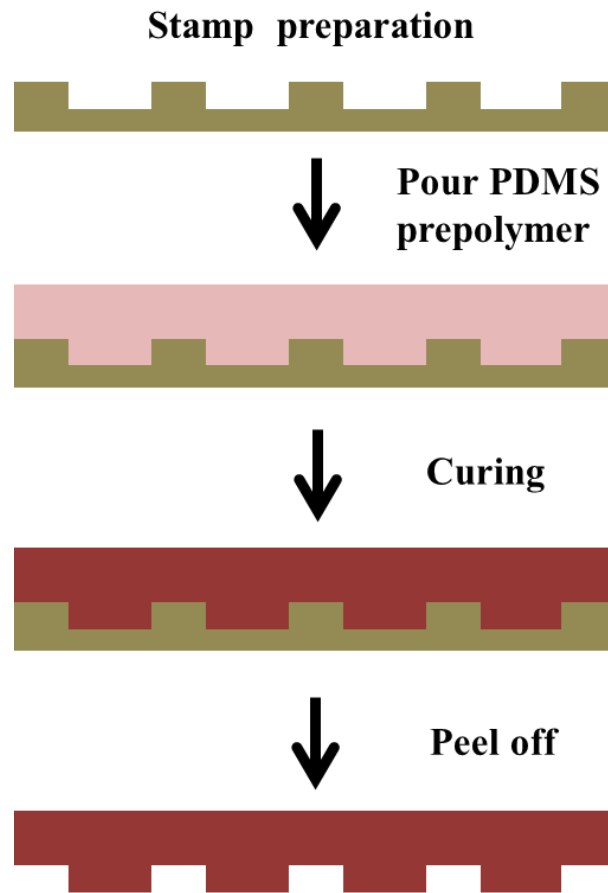
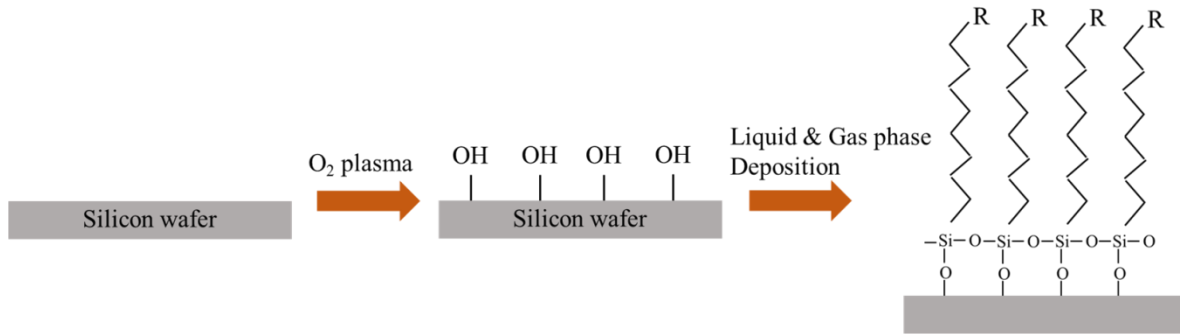


**Figure 1.4** Process of soft lithography

### 1.3.2 Self-Assembled Monolayers (SAMs) treatment

In the soft lithography process, release layer which reduces the surface energy of the stamp and reduces contamination by the resin, is a very important process.<sup>20</sup> The Si substrate used for the master mold has high surface energy, so contamination phenomena due to resin and impurities occur frequently when used without special surface treatment. Therefore, release layer process is necessary to prevent contamination of the stamp during pattern transfer. The release layer treatment is a method of reducing the adhesion of surface by surface treatment. In general, self-assembled monolayers (SAMs) have the advantage that the surface energy can be easily adjusted by using a thin film of several nanometers thick. As shown in Figure 1.5, the basic structure of SAM consists of X group which can be hydrolyzed, linker which became a long alkyl chain, and R which is a functional organic group. The X is a portion mainly reacting with the surface, after being hydrolyzed by water to form a hydroxyl group (-OH), it forms a hydrogen bond with the -OH group on the inorganic surface like silica particles. Also, R group can impart functionality for the next reaction.

a



b

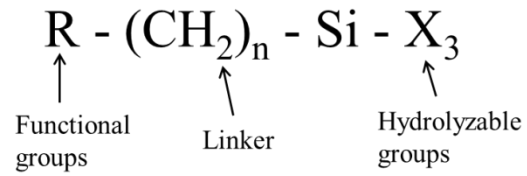


**Figure 1.5** (a) A diagram of deposition of silane SAM on Si wafer, (b) The basic structure of silane coupling agent.

### 1.3.3 Trend of soft lithography

It has been developed several design of the nanostructures as an ARC, such as 1D, 2D diffraction gratings of light incident surface,<sup>21-24</sup> nano-periodic moth's eye structures. Recently, Chen et al. researched an ARC with self-cleaning function using biomimetic moth eye nanostructures by soft nanoimprint lithography.<sup>25</sup> These nanostructures such as nanopillar, nanowires, nanogratings can reduce the surface reflections in wide ranges by the graded effective refractive index. However the fabrication process of master mold are complex and costly such as subsequent dry etching and nanolithography (e.g., laser interference lithography,<sup>26</sup> electron-beamlithography<sup>27</sup>)

In contrast, the master mold with microstructure can be easily fabricated by a cost-effective and relatively simple wet-etching method. The microscale structure can also extend the optical path length and improve the diffuse transmittance, while keeping high total transmittance (e.g., high optical haze).<sup>28-31</sup> Additionally, it can help to lower total internal reflection losses in device.<sup>32-33</sup>

In this thesis, we developed PDMS film with microstructure via simple wet-etching method and soft lithography. The optical properties of PDMS film was investigated, and acquired high optical haze and low reflectance properties as an antireflection layer. Also, the self-cleaning function of the PDMS film was investigated. By applying the PDMS film on two type of solar cells (i.e., Si solar cell and PSC), improved efficiency was compared to solar cells without the PDMS film due to the AR properties. As a result, developed PDMS film is suitable for an antireflection film of all solar cells.

## II. Result and Discussion

### 2.1 Random-Sized Inverted pyramidal structure in PDMS film.

We developed a facile method to fabricate a PDMS film composed of random-sized inverted pyramidal structure (RSIPS) by the soft imprint lithography with a Si mold. Figure 2.1 shows a schematic images of the soft imprint lithography process steps for random sized inverted pyramidal structures (RSIPS) on PDMS films. In advance, Si master molds are fabricated by simple wet-etching method which form the sides of pyramids become randomly, thus resulting in random-sized pyramids (Figure 2.2(a)). As shown in Figure 2.2(a), the average height of the pyramid is  $8\mu\text{m}$ . Then, these random sized pyramidal structure (RSPS) Si master molds are deposited with trichloro-(1H,1H,2H,2H-perfluorooctyl) silane (FOTS). The FOTS monolayer is the hydrophobic region which have function of reduction of surface energy. A prepared PDMS solution was spin-casted on the RSPS-Si mold and cured. The PDMS films were peeled off and thus the PDMS was consisted of RSIPS. It was reported that the light trapping efficiency of random sized pyramid is higher rather than that of uniform sized pyramid by simulation study. Figure 2.2(b) shows the inverted pyramidal structures in the PDMS film were transferred from pyramidal structures of the Si master mold well and the average height of the inverted pyramid on PDMS film is  $5\mu\text{m}$ . Thus, the shape of RSIPS showed the opposite of RSPS Si master mold.



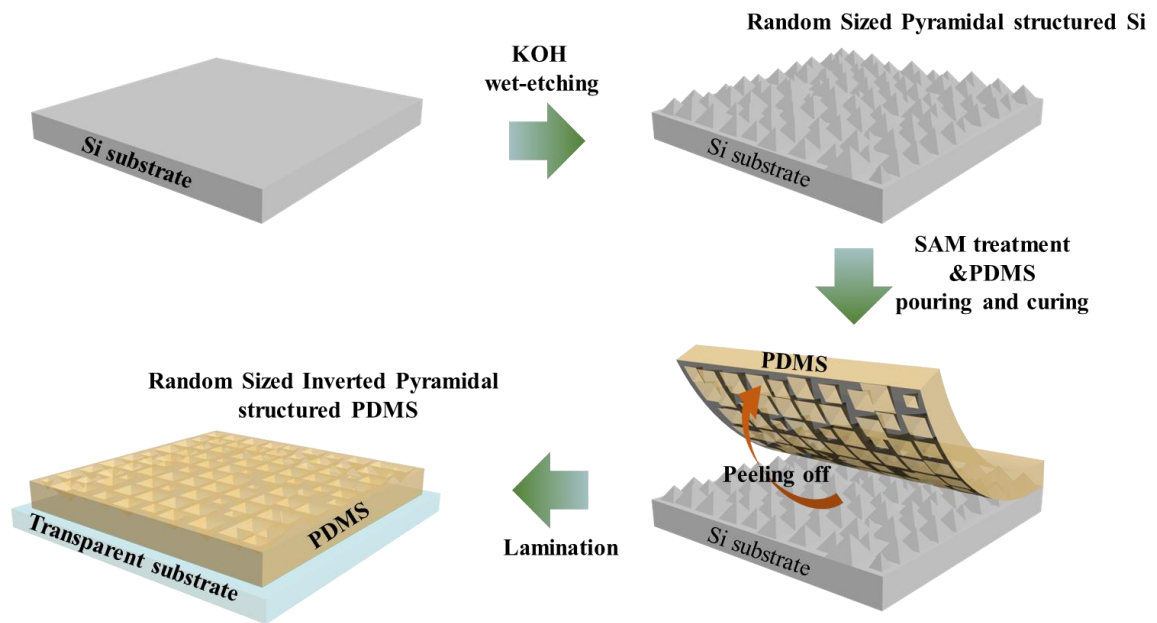


**Figure 2.1** Schematic images of the soft imprint lithography process steps for random sized inverted pyramidal structures (RSIPS) on PDMS films. The RSIPS-PDMS films was laminated on transparent glass substrate.

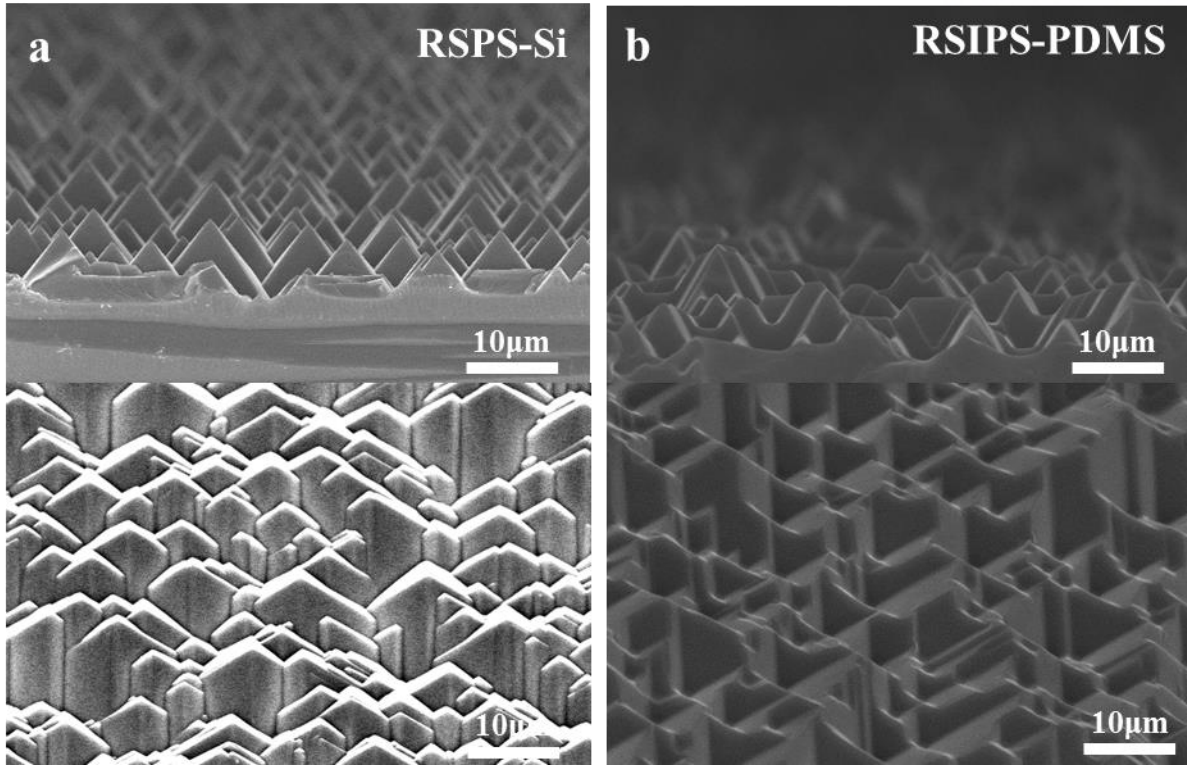


**Figure 2.2** (a) cross-sectional and 30°-tilted view SEM image of the (a) RSPS-Si master mold and (b) RSIPS-PDMS film.

## 2.2. Optical properties

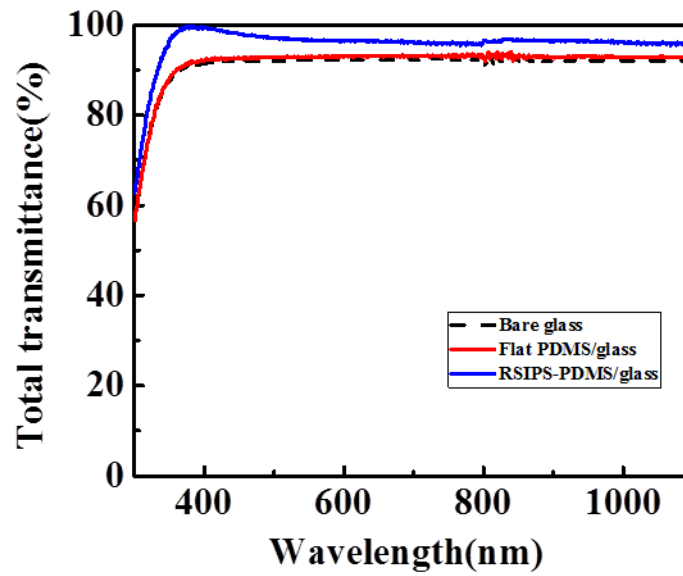
To analyze the optical behaviors of the PDMS films, total transmittance and reflectance spectra were investigated by a UV-Vis/NIR spectrophotometer (Figure 2.3). The result displayed that the total transmittance of flat PDMS film on the glass ( $T_{avg}=91.72\%$ ) was increased compared to the glass ( $T_{avg}=90.99\%$ ) because of step gradient refractive index variation. In addition, by introducing flat PDMS film on the glass, the total reflectance was further reduced, exhibiting the average total reflectance of flat PDMS film/glass ( $R_{avg}$ ) of 7.30% which is lower value than that of glass ( $R_{avg}=8.34\%$ ) (Table 1.). The refractive index at a 550nm wavelength of PDMS film ( $n=1.4$ ) is between air ( $n=1$ ) and glass ( $n=1.53$ ), it can reduce the surface reflection (Figure 2.4). Thus, as an effective antireflection single layer, the flat PDMS film could be considered.

The total transmittance of the RSIPS-PDMS/glass ( $T_{avg}=95.84\%$ ) was higher than that of the flat PDMS film/glass ( $T_{avg}=91.72\%$ ). Also, the RSIPS-PDMS film attached to the glass, causing the reflectance to decrease (i.e.,  $R_{avg}=4.33\%$ ), as shown in Figure 3(b). The effective refractive index ( $n_{eff}$ ) of the RSIPS-PDMS film can be acquired as follows:

$$n_{eff} = \sqrt{[n_{PDMS}^2 \times f + n_{air}^2(1 - f)]}$$

In this equation,  $n_{air}$  and  $n_{PDMS}$  are refractive indexes of the air and PDMS film, and  $f$  is the filling factor of random sized inverted pyramidal structures in PDMS film. The filling factor is speculated from the SEM image of RSIPS-PDMS film (Figure 2.3), and the filling factors are from 0 to 1, respectively, because it varies with the depth. The RSIPS-PDMS film act as a graded layer, mitigating the radical change in the refractive index from the air to PDMS film, as shown in Figure 2.4. Thus, by a linear grading of the effective refractive index profile between the air and glass, the RSIPS-PDMS film shows the lowest reflection.

**a**



**b**

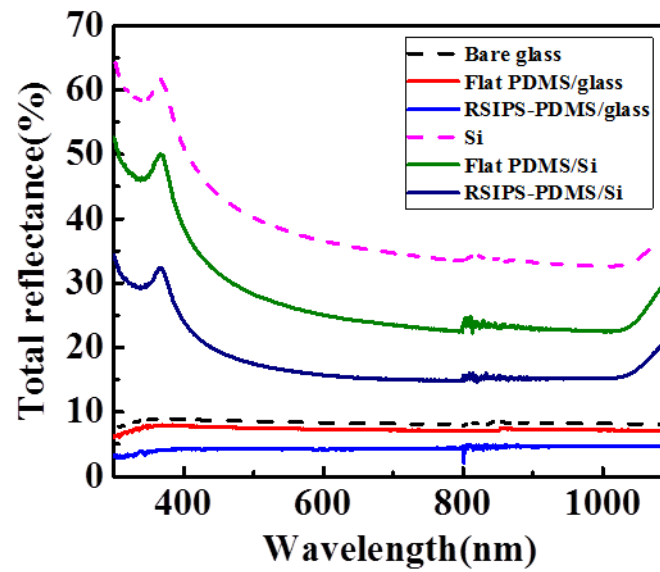


**Figure 2.3** (a) Total transmittance and (b) total reflectance of the flat PDMS film, RIPS-PDMS film on glass or Si wafer.

**Table 1.** The value of the average total transmittance and reflectance over wavelength range of 300-1100nm

	Total transmittance [%]	Total Reflectance [%]
Glass	90.99	8.34
Flat PDMS/glass	91.72	7.30
RSIPS-PDMS/glass	95.84	4.33
Si wafer	-	38.99
Flat PDMS/Si wafer	-	28.01
RSIPS-PDMS/Si wafer	-	18.05

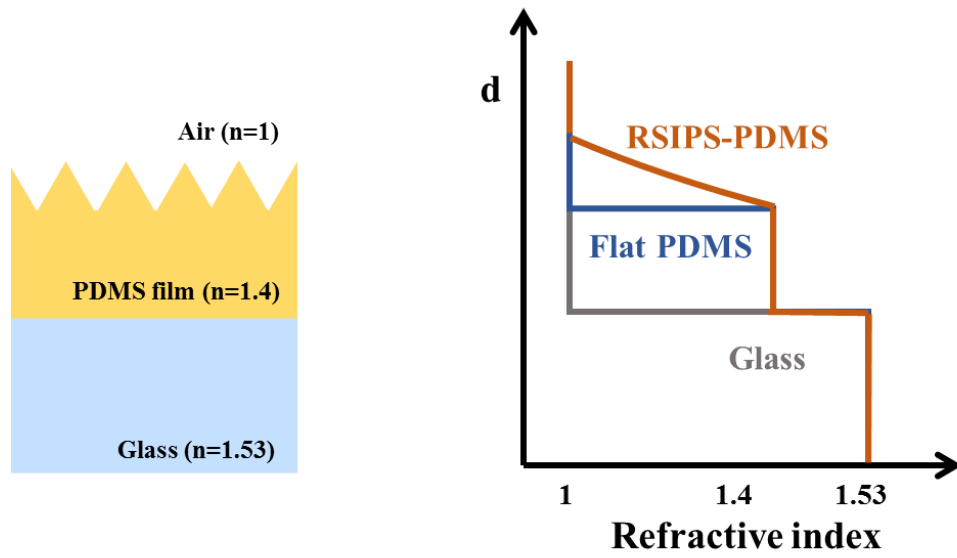


**Figure 2.4** Structure and the variation in refractive index profile with respect to the film depth.

To investigate the influence of the solar power harvest, the calculation of a solar weighted transmittance (SWT) is also important. The SWT is the ratio of the usable photons that have passed to the total usable photons. It can be estimated by the normalizing the transmittance spectra and the solar spectral photon flux (AM1.5G) integrated over a wide wavelength range of 350-800nm. The equation is given by:

$$SWT = \frac{\int_{350nm}^{800nm} I_s(\lambda)T(\lambda)d\lambda}{\int_{350nm}^{800nm} I_s(\lambda)d\lambda}$$

where  $T(\lambda)$  is the total transmittance and  $I_s(\lambda)$  is a spectral intensity of the AM1.5G solar spectrum. The SWT of the bare glass was approximately 92.04%, whereas the SWT of the flat-PDMS film/glass increased to 92.8%. Finally, the SWT increased to 96.91% when the RSIPS-PDMS film attached to the glass. Similarly, from the SWT equation, the solar weighted reflectance (SWR) can be also calculated by replacing the  $T(\lambda)$  with the total reflectance ( $R(\lambda)$ ). As expected, for RSIPS-PDMS film /glass, the SWR value of 4.22% was lower than those for the other surfaces (SWR of the bare glass is 8.41% and SWR of the flat PDMS film/glass is 7.39%).

For the light scattering effect of RSIPS-PDMS film, we observed the logo image as seen through a RSIPS-PDMS film, from Figure 2.5. Figure 2.5(a) show a schematic diagram and (b) displayed photograph of the RSIPS-PDMS film, when the film is positioned between the logo image and the camera. We examined the distinct image due to the excellent optical transparency of the film, when the film is located right on top of the logo image (Figure 2.5(i)). Figure 5(b)(ii) and (iii) show cloudy due to the highly scattered transmitted light through the film, when the film was lifted off from the logo image. Also, the light scattering effect is visualized in Figure 2.6 A green laser beam with a wavelength of 532nm passes through the film and the beam irradiated onto the white paper. The green laser beam is highly scattered and forms a large illuminated rectangular area on the surface (Figure 2.6(b)). When the film is 10 cm away from the screen, you can see that the light is spreading about 6 cm on the screen. Therefore, the angle of light spread is 31 degrees and the path length increases by 1.17 times.

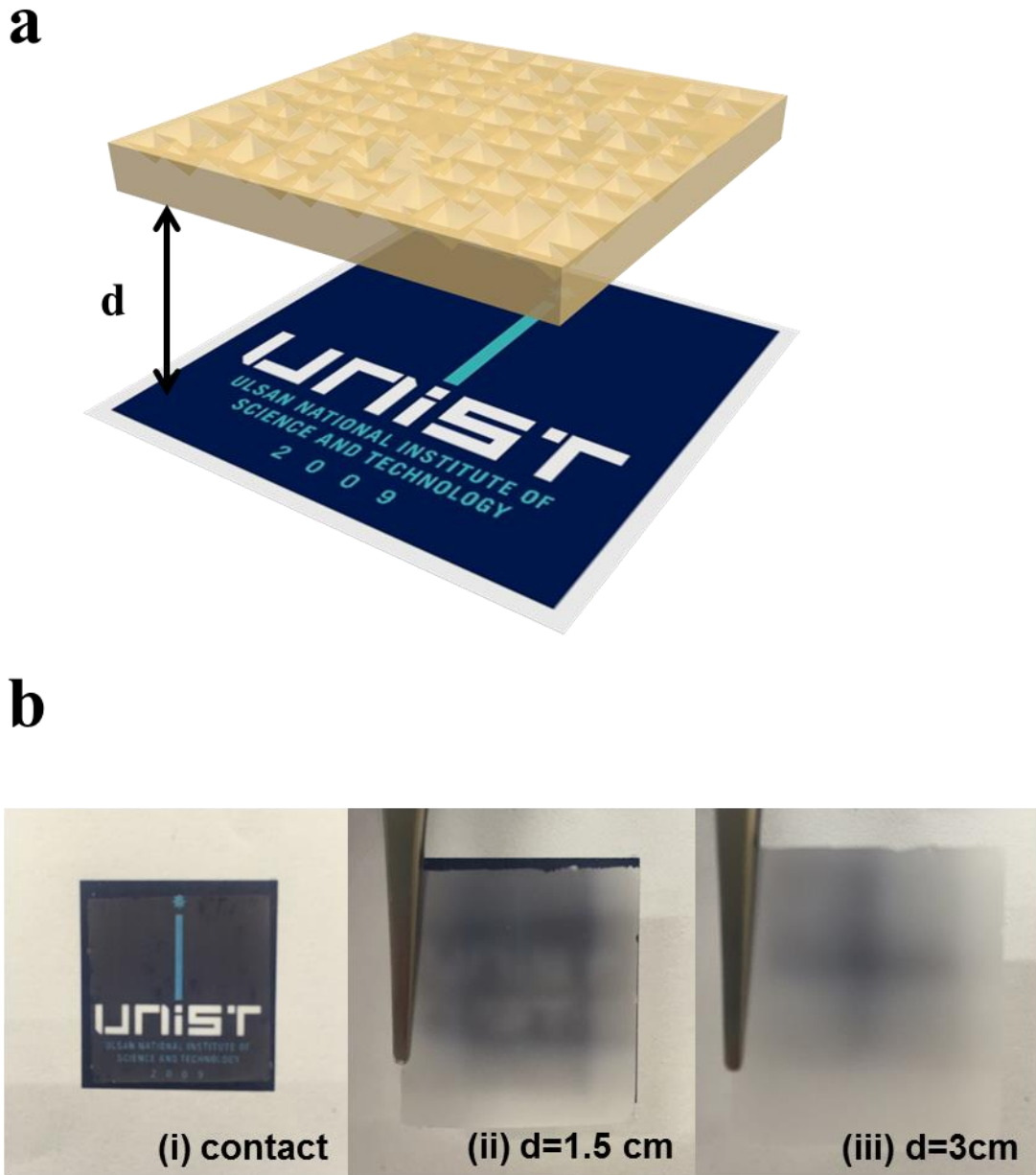
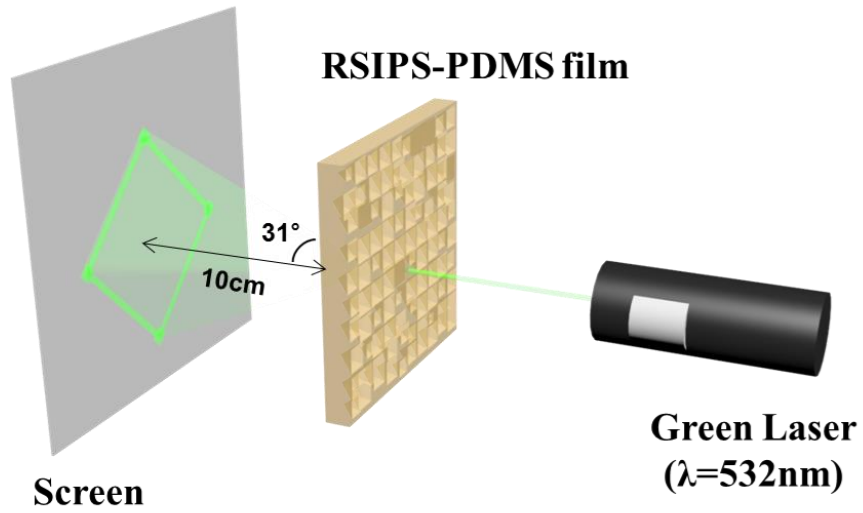


**Figure 2.5** (a) Schematic diagraming and (b) photographs display the logo image as seen through a RSIPS-PDMS film.



**a**



**b**

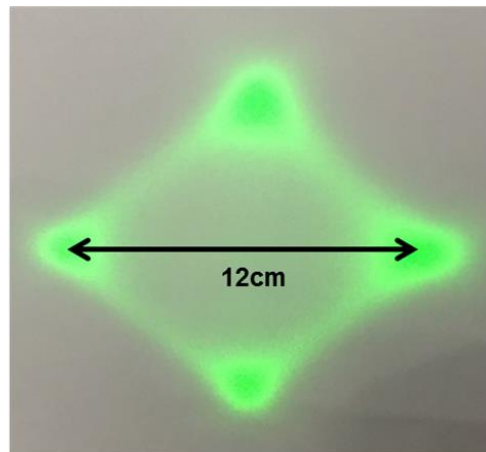


**Figure 2.6** (a) Schematic illustration to show the light scattering effect of RSIP-PDMS film when a laser beam( $\lambda=532\text{nm}$ ) passes through the RSIPS-PDMS film. (b) Photo of diffused light.

The bare glass and flat PDMS film/glass showed very low diffuse transmittance of < 3% in the wide range of wavelengths, as shown in Figure 2.7. Instead, for RSIPS-PDMS film, a tremendous increase in the diffuse transmittance was found, exhibiting an average diffuse transmittance of 96.7% over a broad wavelength range of 300-800nm. This is the reason why the great light scattering is related to higher order diffractions in RSIPS with a larger period than incident light wavelengths. To analyze the light scattering properties of the films, we calculated the haze ratio (H) and it is defined by:

$$H(\%) = \frac{T_d}{T_t} \times 100$$

where  $T_d$  is the diffuse transmittance and  $T_t$  is the total transmittance. For RSIPS-PDMS film/glass, an average H (i.e.,  $H_{avg}=97.36\%$ ) is even higher than that of glass and flat PDMS film/glass (i.e.,  $H_{avg}=0.85\%$  and  $1.07\%$ , respectively). Thus, the rebound and diffracted lights in RSIPS lead to tremendous light scatterings. The light scattering effect can improve the path of light passing in solar cell, which enhance light absorption.

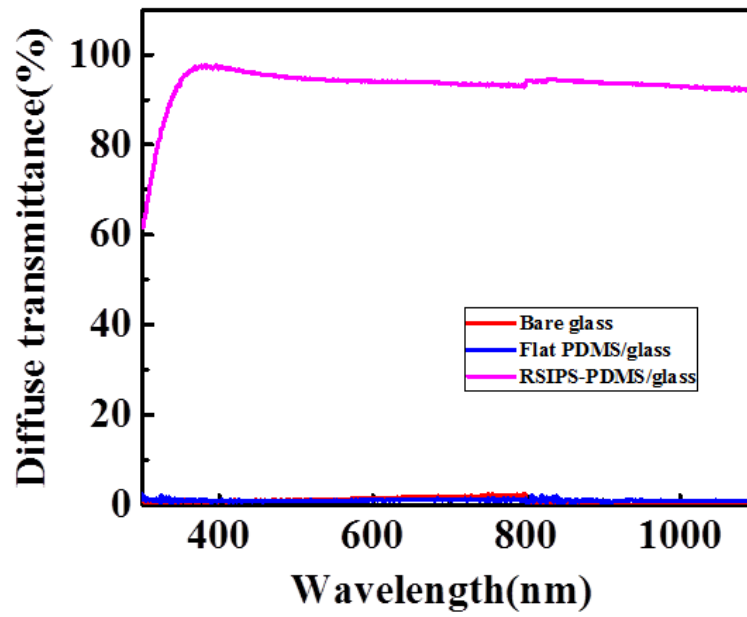


**Figure 2.7** Diffuse transmittance of the samples (bare glass, RSIPS-PDMS film/glass, flat PDMS film/glass)

### 2.3 Surface wettability and self-cleaning effect

To investigate the wetting behavior, we measured the contact angle on the diverse surface type (i.e., bare glass, flat PDMS film, RSIPS-PDMS film). While the bare glass showed a hydrophilic characteristic (i.e., water contact angle ( $\theta_{CA}$ )  $\approx 43^\circ$ ), the flat PDMS film showed a hydrophobic characteristic ( $\theta_{CA} \approx 93^\circ$ ), as shown in Figure 2.8. In particular, for the RSIPS-PDMS film, the hydrophobicity was increased ( $\theta_{CA} \approx 97^\circ$ ). The Cassie-Baxter theory explained the effect is due to the high surface roughness of the PDMS films.<sup>34</sup>

Figure 2.9 also shows the self-cleaning function of RSIPS PDMS film compared to bare glass. The black charcoal particles on the bare glass were still remained after dropping the water droplets due to hydrophilic property of glass. On the other hand, the particles on the RSIPS-PDMS film were relatively cleared removed by flowing water droplet due to hydrophobicity of the film. Thus, a solar cell with this RSIPS-PDMS film is more efficient than that without RSIPS-PDMS film under the outdoor environment such as rain, wind, dust.

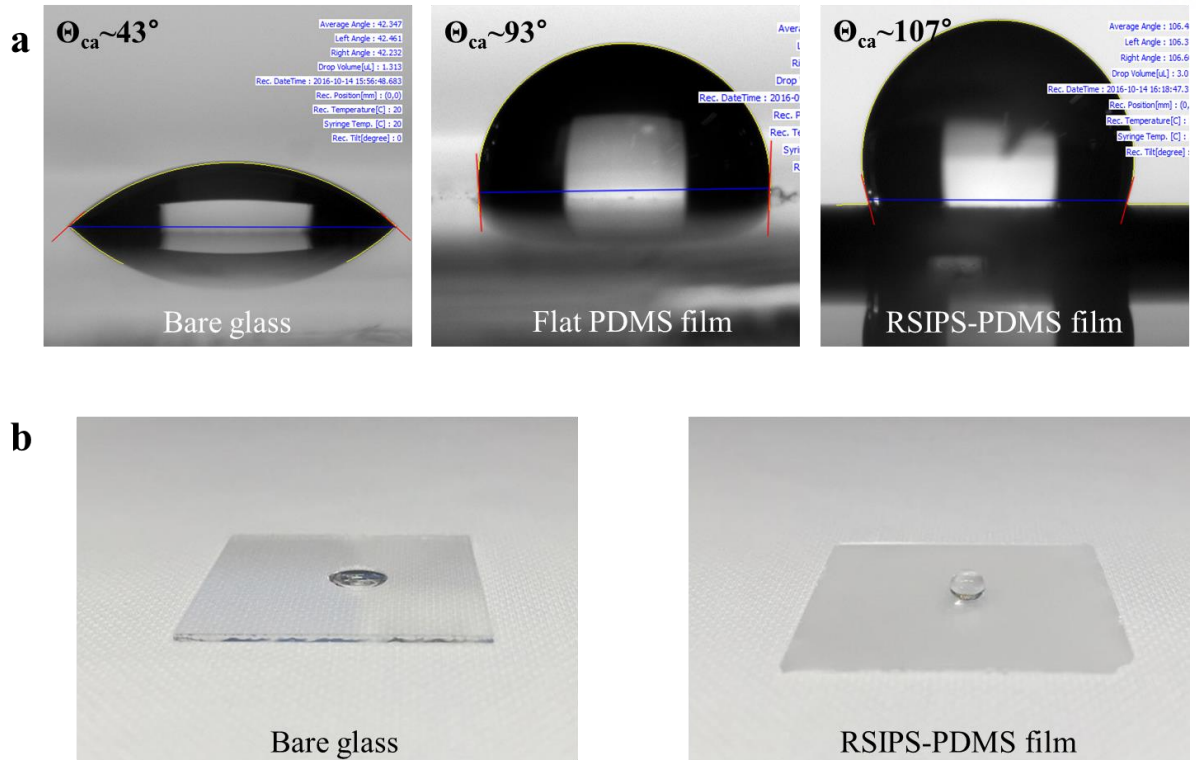


**Figure 2.8** (a) Images show the contact angle of the bare glass, flat PDMS film and RSIPS-PDMS film. (b) Photographs of shape for a water droplet on the substrate (bare glass, RSIPS-PDMS film)

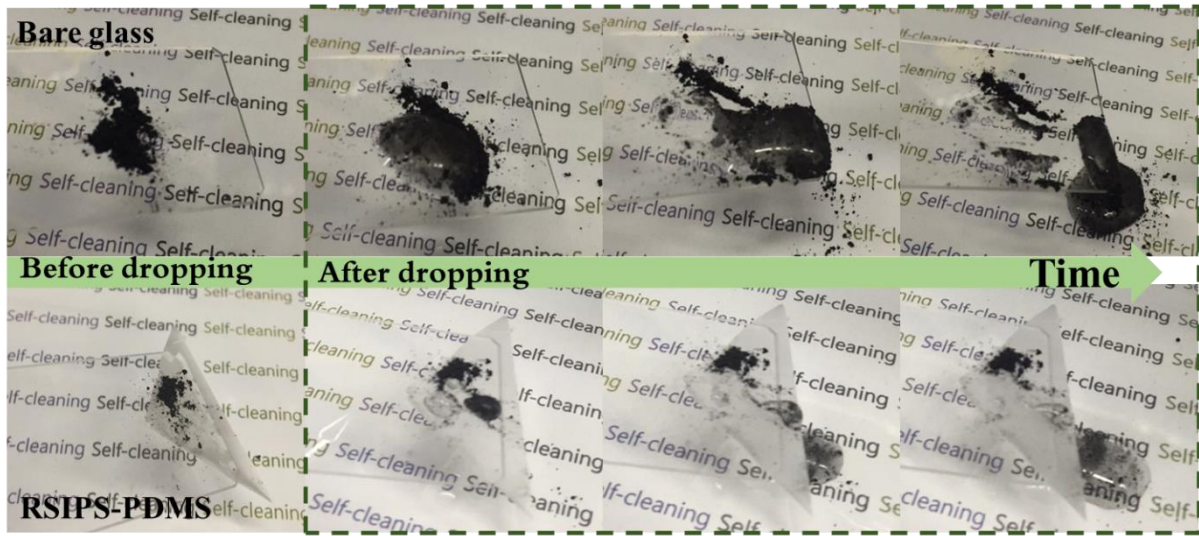


**Figure 2.9** Water droplet self-cleaning behavior of RSIPS-PDMS film compared to bare glass

## 2.4 Characteristics of the Polymer solar cells

We laminate the RSIPS-PDMS film onto the surface transparent substrate with PTB7:PC70BM-based polymer solar cells (PSCs) to utilize high scattering ability and the low reflectance of the RSIPS-PDMS film. To analyze and confirm the effect of the RSIPS-PDMS film on PSCs, we compared to without PDMS film on PSCs, with the flat PDMS film on PSCs, with the RSIPS-PDMS film on PSCs as shown in Figure 2.10. Figure 2.11 shows the representative current density-voltage (J-V) curve of the PSCs without PDMS film, with flat PDMS film, and with the RSIPS PDMS film. The PSC without PDMS film exhibited a PCE of 7.02% using the following parameters:  $V_{oc}=0.730V$ ,  $J_{sc}=14.0\text{mA}/\text{cm}^2$ , and  $FF=68.8\%$  (Table 2). Alternatively, the device with flat PDMS film showed an improved PCE of 7.41% with  $V_{oc} =0.733V$ ,  $J_{sc} =14.77\text{mA}/\text{cm}^2$ , and  $FF=67.8\%$ . The enhancement of  $J_{sc}$  was due to reduced surface Fresnel reflection.

Moreover, compared to the PSC without PDMS film, the PSC with a RSIPS-PDMS film exhibited a much greater PCE of 8.07% with the following parameters:  $V_{oc} =0.733V$ ,  $J_{sc} =16.23\text{mA}/\text{cm}^2$  and  $FF=67.8\%$ . The PCE is enhanced because  $J_{sc}$  of the PSC with RSIPS-PDMS film was higher than that of the PSC without PDMS film. Therefore, this was due to high light scattering property and low reflectance of RSIPS-PDMS film. The calculated photocurrent enhancement factor ( $EF_{j_{sc}}$ ) was 15.9% by the following equation:

$$EF_{j_{sc}} = \frac{\Delta J_{sc}}{J_{sc}} = \frac{J_{sc}(\text{with RSIPS PDMS film}) - J_{sc}(\text{without RSIPS PDMS film})}{J_{sc}(\text{without RSIPS PDMS film})}$$

Additionally, as shown in Fig 2.12(b), EQE measurement proved the enhanced PCE of PSC with RSIPS-PDMS film. The employed RSIPS-PDMS film improved the EQE spectrum from 350 to 800 nm. The EQE spectrum is consistent with the reflectance spectrum. Thus, this represent the broadband antireflection properties for the RSIPS-PDMS film.

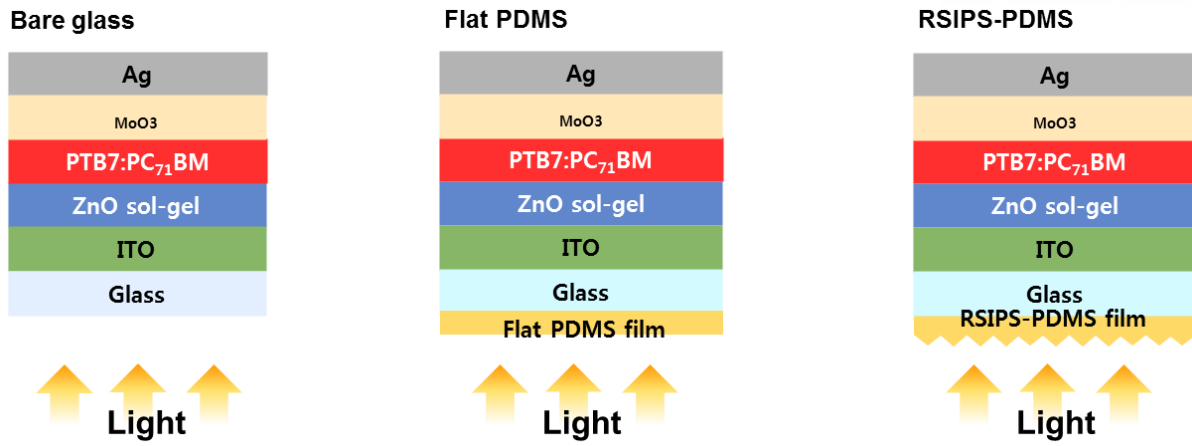


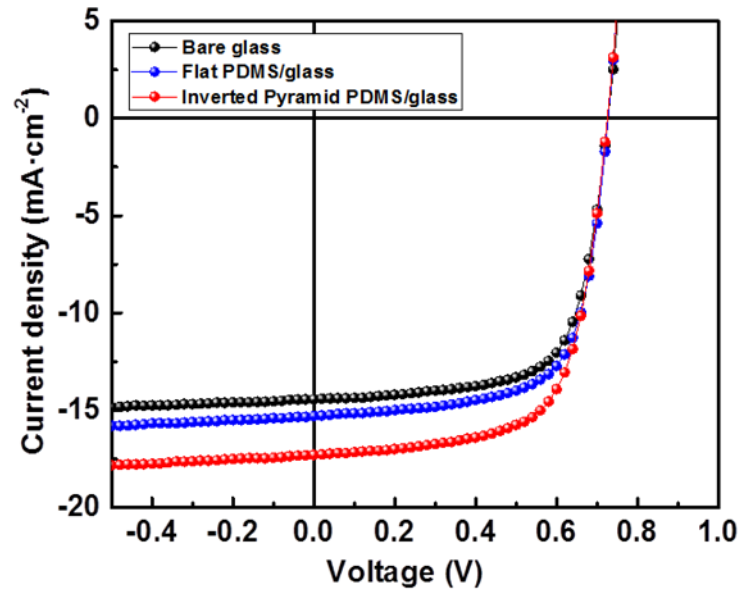
**Figure 2.10** Schematic diagrams of PSC (a)without PDMS film, (b)with flat PDMS film and (c)RSIPS-PDMS film



**Table 2.** Performance of PSCs with the PDMS films

Device	$J_{sc}$ [mA/cm <sup>2</sup> ]	$V_{oc}$ [V]	FF [%]	PCE (best) [%]
Polymer solar cell	14.0	0.730	68.8	7.02(7.23)
Flat PDMS film/Polymer solar cell	14.77	0.733	68.5	7.41(7.63)
RSIPS-PDMS film/Polymer solar cell	16.23	0.733	67.8	8.07(8.48)

a



b

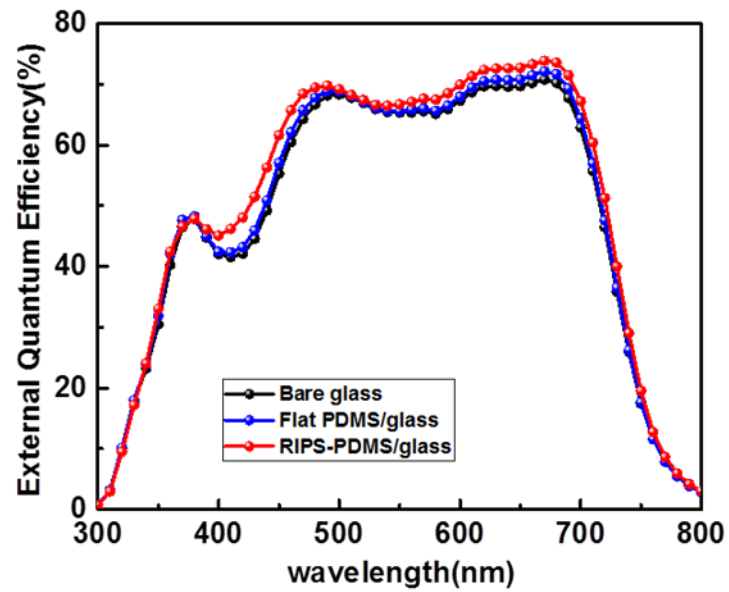


**Figure 2.11**(a) J-V curve of the PSC with diverse film, (b)EQE measurement of PSC with diverse film

## 2.5 Characteristics of the Si solar cells

We also fabricated Si solar cells to apply the RSIPS-PDMS film (Figure 2.12). To analyze and confirm the effect of the RSIPS-PDMS film on Si solar cell, we compared to without PDMS film on Si solar cells, with the RSIPS-PDMS film on Si solar cells.

The J-V curve of Si solar cells with RSIPS-PDMS film were measured as shown in Figure 2.13(a). The values of  $J_{sc}$ ,  $V_{oc}$ , FF, and PCE are summarized in Table 3. The most significant difference between the Si solar cell and Si solar cell with RSIPS-PDMS film is  $J_{sc}$ . For the case of RSIPS-PDMS film on Si solar cell, the increased the  $J_{sc}$  of  $35.9 \text{ mA/cm}^2$  was obtained compared to the reference Si solar cell ( $J_{sc}=33.1 \text{ mA/cm}^2$ ). This means that the RSIPS-PDMS film on the Si solar cell can enhance the light absorption in the device due to reduced reflection of the surface caused by effective refractive index variation from air to Si via inverted pyramid structures. As a result, by laminating the RSIPS-PDMS film on the Si solar cell, the higher PCE of 16% was achieved compared to the reference Si solar cell (PCE=14.9%) due to enhanced  $J_{sc}$ . The use of RSIPS-PDMS film also improved the EQE spectrum of the Si solar cell over a wavelength range of 400-1000nm, as shown in Figure 2.13(b). These increases in EQE spectrum coincide with the reducing tendency in light reflectance, as shown in Figure 2.14(a). Also, Figure 2.14(b) shows similar internal quantum efficiency (IQE) of three type of Si solar cell. Thus, the RSIPS-PDMS film enhanced the  $J_{sc}$ , and increased efficiency of the Si solar cell due to AR property.

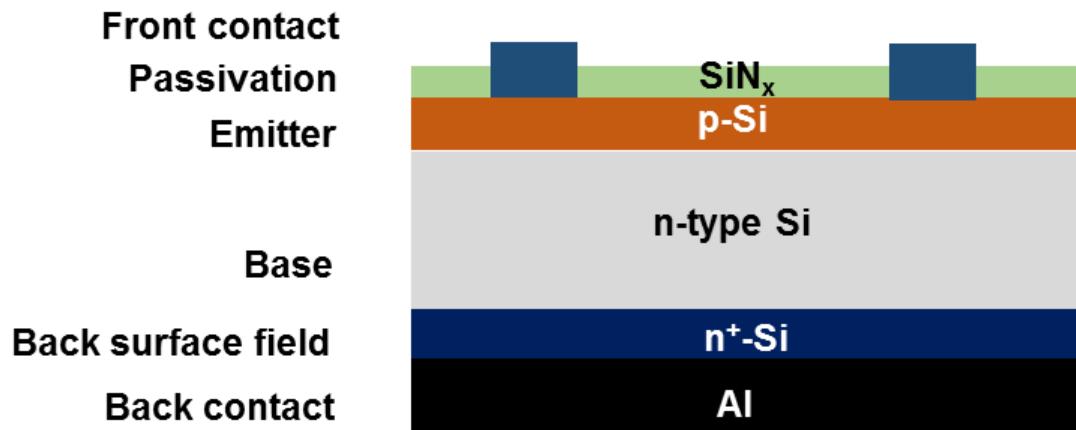
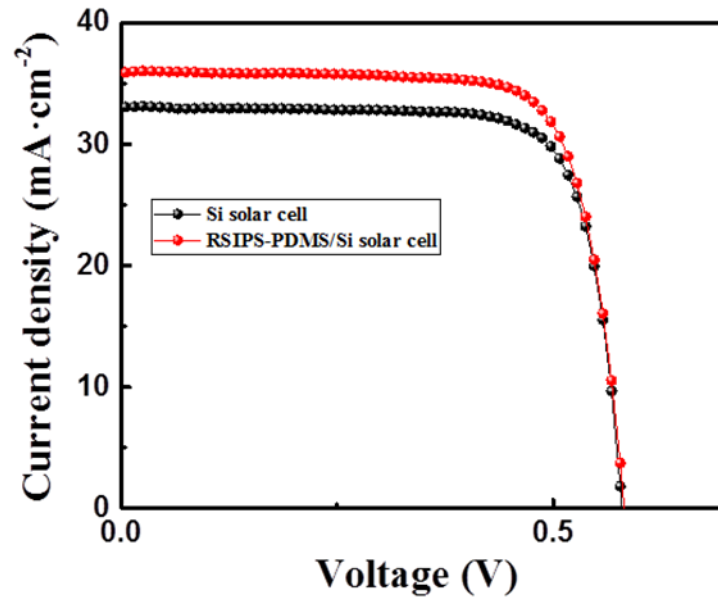


**Figure 2.12** Schematic diagrams of the Si solar cell

**a**



**b**

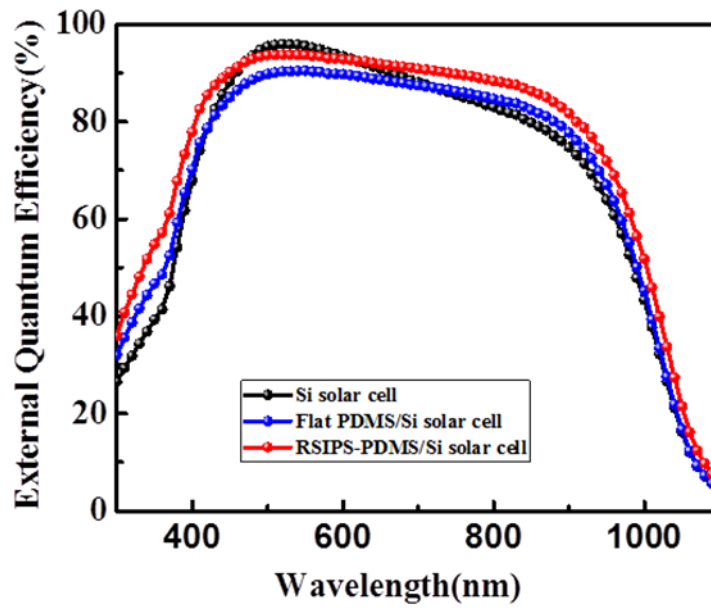
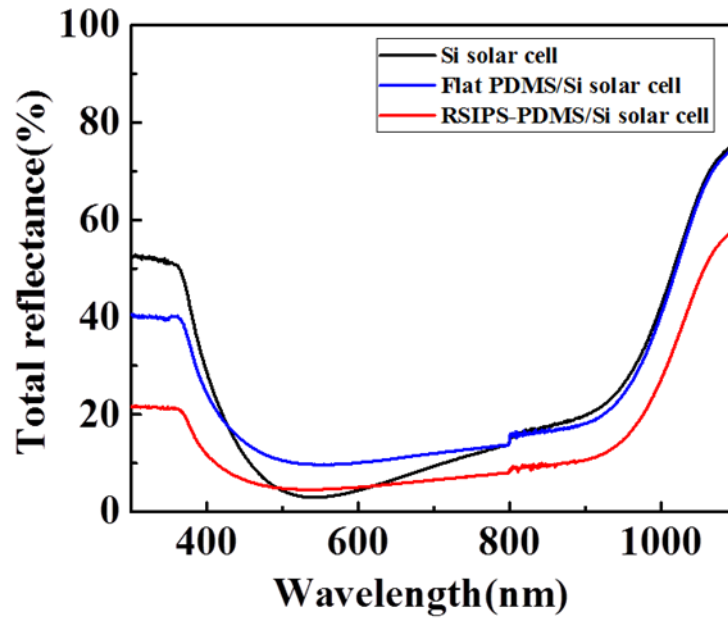


**Figure 2.13** (a) J-V curve and (b) EQE measurement of the Si solar cell

**Table 3.** Performance of Si solar cells

Device	$J_{sc}$ [mA/cm <sup>2</sup> ]	$V_{oc}$ [V]	FF [%]	PCE [%]
Si solar cell	33.1	0.578	77.9	14.9
RSIPS PDMS film/Si solar cell	35.9	0.578	77	16

**a**



**b**

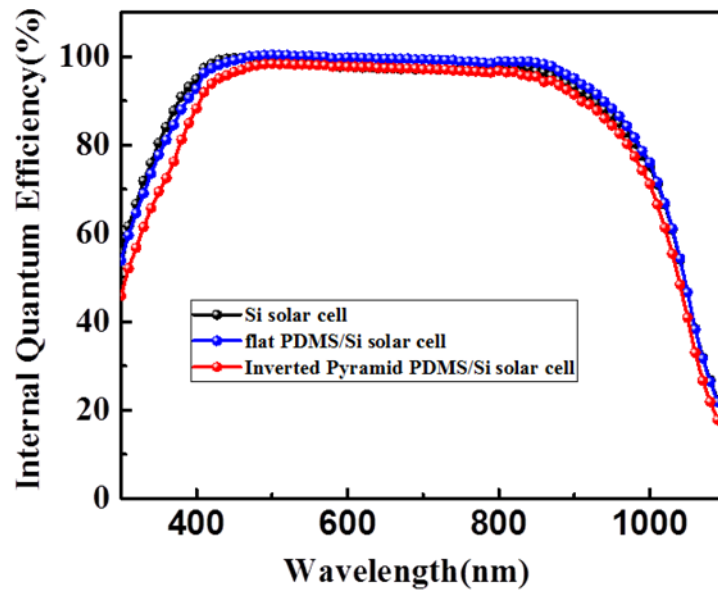


**Figure 2.14** (a) Measured total reflectance and (b) IQE calculation of the Si solar

## 2.6 Conclusion

In summary, we fabricated RSIPS-PDMS film by cost-effective and facile soft lithography using RSPS Si mold formed by simple wet-etching process. The RSIPS-PDMS film on glass represented the excellent optical properties (i.e., SWT=96.91%, SWR=4.22%,  $H_{avg}$ =97.36%) compared to those of glass (i.e., SWT=92.04%, SWR=7.39%,  $H_{avg}$ =0.85%). High transmittance and haze can increase light harvesting in the solar cells. To prove this, the RSIPS-PDMS film was attached on the Si solar cell and PSC. The Si solar cell with RSIPS-PDMS film showed the improved current density and efficiency (i.e., 35.9mA/cm<sup>2</sup>, 16%) compared to those of reference device (i.e., 33.1mA/cm<sup>2</sup>, 14.9%). Likewise, PSC with RSIPS-PDMS film also obtained the enhanced current density and efficiency (i.e., 16.23mA/cm<sup>2</sup>, 8.07%) compared to those of reference device (i.e., 14.0mA/cm<sup>2</sup>, 7.02%). As a result, this thesis proposed the RSIPS PDMS films as an appropriate alternative antireflective layer for every type of solar cells due to facile fabrication process and excellent optical properties.



### III. Experimental Section

#### 3.1 Fabrication of RSPS Si mold

First, to fabricate the RSPS Si mold, the (100) Si wafer was cleaned using acetone, isopropyl alcohol (IPA), and de-ionized (DI) water in consecutive order with sonication for 10minutes each, and was dried by nitrogen (N<sub>2</sub>) gas blow. And then, the Si substrate was immersed in buffer oxide etchant (BOE), 5 wt% hydrofluoric (HF) acid solutions, and DI water for 1 min. Finally, using prepared solution in which IPA, KOH and Di water were mixed in a ratio of 0.5 : 1 : 8.5 vol%, the Si wafer was wet-etched at 75 °C for 40min. In order to eliminate the remaining impurities, the substrate was dipped in a solution mixture of H<sub>2</sub>O<sub>2</sub> : HCl : H<sub>2</sub>O = 1 : 1 : 5 at 80°C for 10min

#### 3.2 Fabrication of RISPS-PDMS film

Prior to fabrication of RISPS-PDMS film, the RSPS Si mold was deposited with trichloro (1H,1H,2H,2H-perfluorooctyl) silane (FOTS) which is one type of silane-coupling agent at 100°C for 900sec. The RSPS Si mold surface have relatively high surface energy with a contact angle of 47° before FOTS treatment. However the FOTS-treated RSPS Si mold has a contact angle of 108° and become a hydrophobic surface, as shown in Figure 3.1. A prepared PDMS solution which composed of mixture of curing agent and base resin with 1 : 10 weight ratio was spin-casted on FOTS treated RSPS Si mold at the spin speed of 500rpm for 30s and cured at 80 °C for 6h in dry oven. The RISPS-PDMS film was finally fabricated by peeling off the PDMS film from the RSPS Si mold.

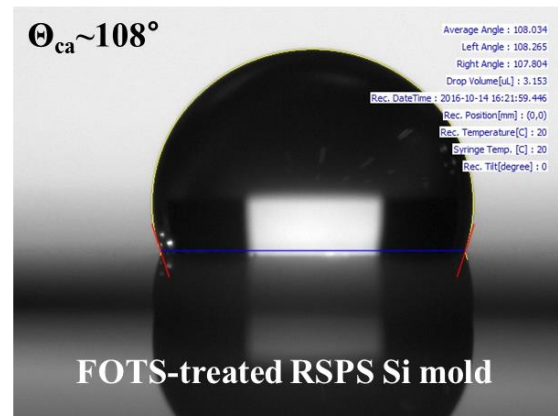
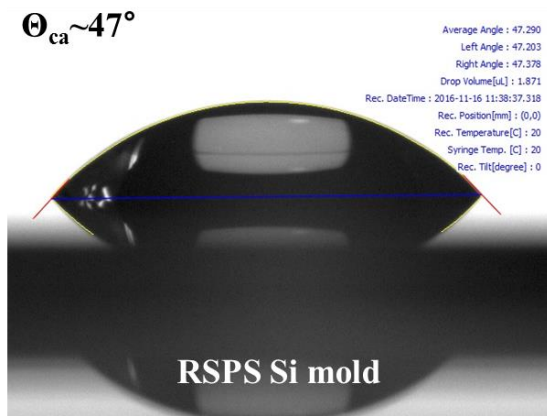


**Figure 3.1** Contact angle of RSPS Si mold and FOTS-treated RSPS Si mold.

### 3.3 Fabrication of polymer solar cells

Prepared the ITO-coated glass substrate was cleaned in acetone, IPA, DI water by ultra-sonication for 10 min. The cleaned ITO-coated glass was treated with a UV-ozone for 30 min. To form a electron transport layer, ZnO sol-gel was prepared by mixing 5 g of 2-methoxyethanol, 0.25 g of ethanol-amine and 0.82 g of zinc acetate and stirring for 1h. The prepared ZnO sol-gel was spin-coated on UV-ozone treated ITO-coated glass at 3000 rpm for 30 s, and annealed at 180°C for 10 min in air. To obtain an active layer which composed of electron donor and acceptor material, 4 mg of PTB7 and 8 mg of PC71BM (1-Material Chemscitech) were dissolved in 0.485ml of chlorobenzene added 0.015 ml of 1,8-diiodooctane. The active material was stirred for 13 h at 60 °C in a nitrogen glove box. To creat active layer, the active solutions were filtered by a 0.45 μm polytetrafluoroethylene syringe filter, and then spin-coated on ZnO layer at 1200 rpm for 60 s. To creat a hole transport layer and electrode, MoO<sub>3</sub> layer (3.8 nm) and Ag layer (70 nm) were evaporated by thermal evaporator. The device area was 0.13 cm<sup>2</sup>

### 3.4 Fabrication of Si solar cells

An emitter layer and back surface field (BSF) layer were created on Si wafer (n-type, 200 μm-thick, 1-3 Ω cm) via the spin-on-dopant (SOD) method. For the BSF layer, the phosphorus dopant source (P509, Filmtronics, Inc.) was spin-coated on a dummy Si wafer, and then baked at 200 °C for 20 min. The diffusion doping was performed in a tube furnace under a mixed ambient of 125 sccm of O<sub>2</sub> and 500 sccm of N<sub>2</sub> at 850 °C. The Si substrate was placed so as to face a dummy wafer coated with phosphorus for formation of a uniform BSF layer on the back side of the Si substrate. Phosphorus glass remaining after SOD diffusion was removed by dipping a diluted HF solution. Next, for the emitter layer, a Boron dopant source (B155, Filmtronics, Inc.) was formed on the front side of Si substrate. It was spin-coated on a dummy Si wafer and baked at 200 °C for 20 min. In the tube furnace, the Si substrate was doped with boron at 850 °C. As a surface passivation, a Al<sub>2</sub>O<sub>3</sub> layer with 10 nm-thick was formed by atomic layer deposition on the emitter after eliminating the boron glass and silicon oxide. For creating the micro-grid electrode, the Si wafer was spin-coated with photoresist (AZ4330, AZ electronic materials). Al layer were evaporated with 500 nm-thick on the front and back side of the substrate by a thermal evaporator. Lastly, the photoresist was eliminated by using acetone solution. This device area was 1 cm<sup>2</sup>

## References

1. Chu, Y.; Meisen, P., Review and comparison of different solar energy technologies. *Global Energy Network Institute (GENI), San Diego, CA* **2011**.
2. Srinivas, B.; Balaji, S.; Nagendra Babu, M.; Reddy, Y., Review on Present and Advance Materials for Solar Cells. *International Journal of Engineering Research-Online* **2015**, *3*, 178-182.
3. Choubey, P.; Oudhia, A.; Dewangan, R., A review: Solar cell current scenario and future trends. *Recent Research in Science and Technology* **2012**, *4* (8).
4. Rayleigh, L., On reflection of vibrations at the confines of two media between which the transition is gradual. *Proceedings of the London Mathematical Society* **1879**, *1* (1), 51-56.
5. Kim, S. W.; Bae, D.-S.; Shin, H., Zinc-embedded silica nanoparticle layer in a multilayer coating on a glass substrate achieves broadband antireflection and high transparency. *Journal of applied physics* **2004**, *96* (11), 6766-6771.
6. Leem, J.; Song, Y.; Lee, Y.; Yu, J., Effect of etching parameters on antireflection properties of Si subwavelength grating structures for solar cell applications. *Applied Physics B* **2010**, *100* (4), 891-896.
7. Macleod, H., Thin optical filters. *London Adam Hilger* **1986**.
8. Raut, H. K.; Ganesh, V. A.; Nair, A. S.; Ramakrishna, S., Anti-reflective coatings: A critical, in-depth review. *Energy & Environmental Science* **2011**, *4* (10), 3779-3804.
9. B. Dale, H. G. R., High efficiency silicon solar cells. *In: Proceedings of the 14th Annual Power Sources Conference*. **1960**, 22.
10. Sun, C.-H.; Jiang, P.; Jiang, B., Broadband moth-eye antireflection coatings on silicon.

*Applied Physics Letters* **2008**, 92 (6), 061112.

11. Min, W. L.; Jiang, B.; Jiang, P., Bioinspired Self-Cleaning Antireflection Coatings. *Advanced Materials* **2008**, 20 (20), 3914-3918.
12. Huang, J.; Wang, X.; Wang, Z. L., Bio-inspired fabrication of antireflection nanostructures by replicating fly eyes. *Nanotechnology* **2007**, 19 (2), 025602.
13. Diedenhofen, S. L.; Vecchi, G.; Algra, R. E.; Hartsuiker, A.; Muskens, O. L.; Immink, G.; Bakkers, E. P.; Vos, W. L.; Rivas, J. G., Broad-band and Omnidirectional Antireflection Coatings Based on Semiconductor Nanorods. *Advanced Materials* **2009**, 21 (9), 973-978.
14. Tao, M.; Zhou, W.; Yang, H.; Chen, L., Surface texturing by solution deposition for omnidirectional antireflection. *Applied Physics Letters* **2007**, 91 (8), 081118.
15. Song, Y. M.; Xie, Y.; Malyarchuk, V.; Xiao, J.; Jung, I.; Choi, K.-J.; Liu, Z.; Park, H.; Lu, C.; Kim, R.-H., Digital cameras with designs inspired by the arthropod eye. *Nature* **2013**, 497 (7447), 95-99.
16. Tsui, K. H.; Lin, Q.; Chou, H.; Zhang, Q.; Fu, H.; Qi, P.; Fan, Z., Low-Cost, Flexible, and Self-Cleaning 3D Nanocone Anti-Reflection Films for High-Efficiency Photovoltaics. *Advanced Materials* **2014**, 26 (18), 2805-2811.
17. Leem, J. W.; Guan, X.-Y.; Choi, M.; Yu, J. S., Broadband and omnidirectional highly-transparent coverglasses coated with biomimetic moth-eye nanopatterned polymer films for solar photovoltaic system applications. *Solar Energy Materials and Solar Cells* **2015**, 134, 45-53.
18. Galeotti, F.; Trespidi, F.; Timò, G.; Pasini, M., Broadband and crack-free antireflection coatings by self-assembled moth eye patterns. *ACS applied materials & interfaces* **2014**, 6 (8), 5827-5834.
19. Leem, J. W.; Kim, S.; Lee, S. H.; Rogers, J. A.; Kim, E.; Yu, J. S., Efficiency Enhancement of Organic Solar Cells Using Hydrophobic Antireflective Inverted Moth-Eye Nanopatterned PDMS Films. *Advanced Energy Materials* **2014**, 4 (8).

20. Dong-Il Lee, K.-D. k., Jun-Ho Jeong, Eung-Sug Lee, Dae-Geun Choi, The Surface Treatment Effect for Nanoimprint Lithography using Vapor Deposition of Silane Coupling Agent. *Korean Chem. Eng. Res.* **2007**, *45* (2), 149-154.
21. Forberich, K.; Dennler, G.; Scharber, M. C.; Hingerl, K.; Fromherz, T.; Brabec, C. J., Performance improvement of organic solar cells with moth eye anti-reflection coating. *Thin Solid Films* **2008**, *516* (20), 7167-7170.
22. Kubota, S.; Kanomata, K.; Ahmmad, B.; Mizuno, J.; Hirose, F., Optimized design of moth eye antireflection structure for organic photovoltaics. *Journal of Coatings Technology and Research* **2016**, *13* (1), 201-210.
23. Choi, S. J.; Huh, S. Y., Direct Structuring of a Biomimetic Anti-Reflective, Self-Cleaning Surface for Light Harvesting in Organic Solar Cells. *Macromolecular rapid communications* **2010**, *31* (6), 539-544.
24. Brongersma, M. L.; Cui, Y.; Fan, S., Light management for photovoltaics using high-index nanostructures. *Nature Materials* **2014**, *13* (5), 451-460.
25. Chen, J. D.; Zhou, L.; Ou, Q. D.; Li, Y. Q.; Shen, S.; Lee, S. T.; Tang, J. X., Enhanced Light Harvesting in Organic Solar Cells Featuring a Biomimetic Active Layer and a Self-Cleaning Antireflective Coating. *Advanced Energy Materials* **2014**, *4* (9).
26. bin Mohd Yusoff, A. R.; Kim, D.; Kim, H. P.; Shneider, F. K.; da Silva, W. J.; Jang, J., A high efficiency solution processed polymer inverted triple-junction solar cell exhibiting a power conversion efficiency of 11.83%. *Energy & Environmental Science* **2015**, *8* (1), 303-316.
27. Che, X.; Xiao, X.; Zimmerman, J. D.; Fan, D.; Forrest, S. R., High-Efficiency, Vacuum-Deposited, Small-Molecule Organic Tandem and Triple-Junction Photovoltaic Cells. *Advanced Energy Materials* **2014**, *4* (18).
28. Janthong, B.; Moriya, Y.; Hongsingthong, A.; Sichanugrist, P.; Konagai, M., Management of light-trapping effect for a-Si: H/ $\mu$ c-Si: H tandem solar cells using novel substrates, based on MOCVD

ZnO and etched white glass. *Solar Energy Materials and Solar Cells* **2013**, *119*, 209-213.

29. Ko, Y. H.; Yu, J. S., Highly transparent sapphire micro-grating structures with large diffuse light scattering. *Optics express* **2011**, *19* (16), 15574-15583.
30. Leem, J. W.; Kim, M. S.; Yu, J. S., Broadband highly transparent sapphires with biomimetic antireflective compound submicrometer structures for optical and optoelectronic applications. *JOSA B* **2013**, *30* (6), 1665-1670.
31. Chen, Y.-P.; Lee, C.-H.; Wang, L. A., Fabrication and characterization of multi-scale microlens arrays with anti-reflection and diffusion properties. *Nanotechnology* **2011**, *22* (21), 215303.
32. Li, K.; Feng, C.; Choi, H., Analysis of micro-lens integrated flip-chip InGaN light-emitting diodes by confocal microscopy. *Applied Physics Letters* **2014**, *104* (5), 051107.
33. Huang, S.-H.; Horng, R.-H.; Wen, K.-S.; Lin, Y.-F.; Yen, K.-W.; Wu, D.-S., Improved light extraction of nitride-based flip-chip light-emitting diodes via sapphire shaping and texturing. *IEEE photonics technology letters* **2006**, *18* (24), 2623-2625.
34. Tserepi, A.; Vlachopoulou, M.; Gogolides, E., Nanotexturing of poly (dimethylsiloxane) in plasmas for creating robust super-hydrophobic surfaces. *Nanotechnology* **2006**, *17* (15), 3977.